Available online at www.sciencedirect.com

SciVerse ScienceDirect

Ceramics International 38 (2012) 3217–3225

CERAMICS INTERNATIONAL

www.elsevier.com/locate/ceramint

Structure stability and microwave dielectric properties of double perovskite ceramics – $Ba_2Mg_{1-x}Ca_xWO_6$ ($0.0 \leq x \leq 0.15$)

Jia Yin Wu, Jian Jiang Bian *

Department of Inorganic Materials, Shanghai University, 149 Yanchang Road, Shanghai 200072, China

Received 1 December 2011; received in revised form 10 December 2011; accepted 10 December 2011
Available online 21 December 2011

Abstract

The structure stability of double perovskite ceramics – $Ba_2Mg_{1-x}Ca_xWO_6$ ($0.0 \leq x \leq 0.15$) has been studied by X-ray powder diffraction (XRD), scanning electron microscopy (SEM) and Raman spectrometry in this paper. The microwave dielectric properties of the ceramics were studied with a network analyzer at the frequency of about 8–11 GHz. The results show that small amount of Ca substitution for Mg increases the Mg/Ca–O bond strength, and hence the stability of the double perovskite. But it cannot completely suppress the decomposition of $Ba_2Mg_{1-x}Ca_xWO_6$ at high temperature. Although space group $Fm\bar{3}m$ is adopted for all compositions, nonrandom distribution of Ca^{2+} and Mg^{2+} on 4b-site within the short range scale is observed due to their large cation size difference. Small level doping of Ca ($x \leq 0.1$) increases the dielectric permittivity monotonically, but does not affect the $Q \times f$ value greatly. As expected, the substitution of Ca tuned the temperature coefficient of resonant frequency (τ_f value) from negative to positive value. Excellent combined microwave dielectric properties with $\varepsilon_r = 20.8$, $Q \times f = 120{,}729$ GHz, and $\tau_f = 0$ ppm/°C could be obtained for $x = 0.1$ composition. However the $Q \times f$ value degrades considerably when the sample was stored under ambient conditions for a long time.

Keywords: Double perovskite; Structure stability; Microwave dielectric properties

1. Introduction

Complex perovskites of the $A^{2+}(B^{2+}_{1/3}B^{5+}_{2/3})O_3$ family (where A = Ba, Sr; B^{2+} = Mg^{2+}, Zn^{2+}; B^{5+} = Ta^{5+}, Nb^{5+}), with partial order in B-site position, have been reported to have exceptionally low-dielectric loss at microwave frequencies [1–3]. A great amount of work has been done on these 1:2 complex perovskite compounds [4–6]. It has been shown that the ultra-low dielectric losses of these materials are closely related to the 1:2 B-site ionic ordering state. Microwave dielectric properties of several 1:1 ordered compounds with the general formula $A(B'_{1/2}B''_{1/2})O_3$ (A = Ba, Sr, Ca; B′ = La, Nd, Sm, Yb; B″ = Ta, Nb) have been investigated by several authors [7–10]. Mixed alkaline earth tungstate double perovskites with the general formula $A(B_{1/2}W_{1/2})O_3$ (A = Ba, Sr, Ca; B = Mg, Co, Zn, Ni) are of interest for their complete 1:1 ordered state due to their larger differences in charge and ionic radii on B-site. The barium containing tungstate double perovskites were determined to be cubic and in the space group $Fm\bar{3}m$. However it is difficult to obtain a pure phase of barium containing tungstate double perovskites. Small amount of scheelite $BaWO_4$ impurity phase usually existed. Single-phase of $Ba(Mg_{1/2}W_{1/2})O_3$ (BMW) could be obtained by precursor method in which wolframite $MgWO_4$ was firstly formed and then BMW was synthesized at the temperature approximately 1200 °C by adding stoichiometric amounts of $BaCO_3$. However BMW is unstable at high temperature and $BaWO_4$ impurity phase appears in the sample sintered at the temperature above 1400 °C [11]. The stability of perovskite structure could be evaluated by the so-called global instability index (GII) which is based on differences between experimental and calculated bond valence sums. Crystal structures for which GII > 0.2 are generally unstable [12]. The GII of BMW calculated by SpuDS [13] is 0.34 v.u. at room temperature and 0.71 at 1500 °C, which implies the instability of BMW, especially at high temperature. The thermodynamic instability of BMW could also be understood by comparing the enthalpies of formation for $MeWO_4$ (Me is Mg, Ca, Sr, Ba). The enthalpy increases

* Corresponding author.
E-mail address: jjbian@shu.edu.cn (J.J. Bian).

0272-8842/$36.00
doi:10.1016/j.ceramint.2011.12.027

with the increase of ionic radii of alkaline earth [14]. It means that scheelite $BaWO_4$ is more thermodynamically stable than wolframite $MgWO_4$, which also explained the formation of scheelite $BaWO_4$ impurity phase at high temperature.

Khalyavin et al. [11] and Zhao et al. [15] have reported the microwave dielectric properties of $Ba(B_{1/2}W_{1/2})O_3$ (B = Mg, Ni, Zn) and $A(B_{1/2}W_{1/2})O_3$ (A = Ba, Sr,; B = Co, Ni, Zn), respectively. Microwave dielectric measurement showed that $Ba(Mg_{1/2}W_{1/2})O_3$ (BMW) double perovskite exhibited dielectric properties of ε_r = 15–17.6, $Q \times f$ = 45,200–57,300 GHz, $\tau_f = -25$ ppm/°C. Very high value of $Q \times f \sim 107{,}000$ GHz has been reported by Takahashi et al. [16] for the $(1-x)$BMW–xBaTiO$_3$ system near $x \sim 1/3$. The high $Q \times f$ value was attributed to the stabilization of the 6H hexagonal structure with a high degree of the $Mg^{2+}/(W^{6+}, Ti^{4+})$ ionic ordering [16,17]. Recently, A-site ion substitution effect on the microwave dielectric properties of $A_{1-3x}/2La_x(Mg_{1/2}W_{1/2})O_3$ (A = Ba, Sr, Ca; $0.0 \le x \le 0.05$) double perovskites has been investigated [18]. Bian et al. [18] reported that La-substituted samples maintain the same crystal symmetry as the corresponding unsubstituted samples and that low La-substituted concentration is helpful in avoiding AWO_4 formation and tailoring the microwave dielectric properties. The $Q \times f$ value of the La-doped BMW could be improved to more than 100,000 GHz when $x = 0.02$, but the sintering temperature simultaneously increased to about 1600 °C due to the decrease of $BaWO_4$ impurity phase.

The relations between ionic parameters and intrinsic microwave dielectric properties have been investigated by IR spectrum study for the $Ba(B'_{1/2}B''_{1/2})O_3$ complex perovskite ceramics [19]. Ionic size, manifesting itself in tolerance factor (t), is found to be the most important parameter in controlling the intrinsic microwave dielectric properties. For $t > 1$ (BMW: t = 1.034) B′-site cations have too much room, resulting in an increasing of damping of the second mode involving B′-site cation vibration. Damping could be minimized by changing the ionic size to fulfill $t \sim 1$.

Based on the aforementioned consideration, we choose larger sized Ca^{2+} as dopant partially substituting for Mg^{2+} so as to reduce the tolerance factor. On the other hand, Ba_2CaWO_6 was reported to have positive τ_f value (+46 ppm/°C) [20], thus near zero τ_f value is expected to be tuned for Ba_2MgWO_6 by the doping of Ca^{2+} on Mg-site. As reported, $Ba_2Mg_{1-x}Ca_xWO_6$ series shows a broad miscibility gap from $x \sim 0.3$ to ~ 0.8 [21]. Therefore, we limited the maximum doping concentration to $x = 0.15$ in our experiment. Crystal structure, microstructure and microwave dielectric properties of $Ba_2Mg_{1-x}Ca_xWO_6$ ceramics were investigated in the present paper. The perovskite structural stability and its influence on the microwave dielectric properties of $Ba_2Mg_{1-x}Ca_xWO_6$ were discussed.

2. Experimental

$Ba_2Mg_{1-x}Ca_xWO_6$ ($0.0 \le x \le 0.15$) ceramics were prepared by a conventional solid-state reaction route. High purity $BaCO_3$ (99.7%), MgO (99.7%), $CaCO_3$ (99.5%) and WO_3 (99.5%) were used as raw materials. The compounds were weighed according to the above formula and mixed with ZrO_2 balls in ethanol for 24 h, dried and calcined at the temperature of 1200 °C for 2 h in alumina crucible. The calcined powders were pulverized again by ball milling in ethanol for 24 h. After drying, mixed with 7–10 wt.% PVA and sieving, the granulated powders were uniaxially pressed into compacts 10 mm in diameter and 4.5 mm thickness under a pressure of 120 MPa. The compacts were sintered at 1450 °C–1550 °C for 2 h. The sintering temperature was optimized by the maximum bulk density and $Q \times f$ value.

The phase constituents of the sintered samples were identified by X-ray diffraction (XRD) with Ni-filtered Cu Kα radiation (Rigaku D\max 2200, Tokyo, Japan). The content of $BaWO_4$ phase in each specimen was estimated from the reflection intensities via Jade 6.5 software. For Rietveld refinement of the X-ray patterns, the powder diffraction data were collected at room temperature with a step size $\Delta 2\theta = 0.02°$ over the angular range $5 \le 2\theta\ (°) \le 135$ using monochromatic Cu Kα1 radiation (40 kV, 250 mA). The obtained data were refined by the Rietveld method using the Fullprof program. The Raman spectra were carried out for the sintered samples (RENIShaw in Via plus, UK). The Raman spectra were excited with the 785 nm line of a semiconductor laser at a power of 250 mW and recorded in back-scattering geometry using InVia Raman microscope equipped with a grating filter, enabling good stray light rejection in the 100–1000 cm range. The microstructure of the sintered sample was characterized by scanning electron microscopy (SEM) (Apollo300, CamScan, U.K.). The samples were polished and thermally etched at a temperature of 100 °C lower than the sintering temperature for 30 min. Chemical compositions were analyzed by energy dispersive spectrometer (EDS) (INCA EDS, OXFORD, UK). Microwave dielectric properties of the sintered samples were measured between 7 GHz and 13 GHz using network analyzer (N5230A, Agilent, Palo Alto, CA, USA). The quality factor was measured by the transmission cavity method. The relative dielectric constant (ε_r) was measured according to the Hakki–Coleman method using the TE_{011} resonant mode, and the temperature coefficient of the resonator frequency (τ_f) was measured using invar cavity in the temperature range from 20 °C to 80 °C.

3. Results and discussion

Fig. 1 shows the powder XRD patterns of $Ba_2Mg_{1-x}Ca_xWO_6$ sintered at 1500 °C/2 h. The lack of peak splitting confirmed that all the compounds exhibited cubic perovskite structure and could be indexed in the space group $Fm-3m$. The large intensity at (1 1 1) reflection indicates ordering of the B-site cations. It is noted that the peak positions shift to lower 2θ degree with the increase of x, which means the cell volume increases with increasing x due to the substitution of larger Ca^{2+} (R = 1.0 Å) for smaller Mg^{2+} (R = 0.72 Å). Small amount of impurity $BaWO_4$ phase could be detected from the XRD patterns of all compositions. Variation of $BaWO_4$ content with x is shown in Fig. 2. It decreases with increasing x and reaches minimum at $x = 0.1$, subsequent increase in x increases the

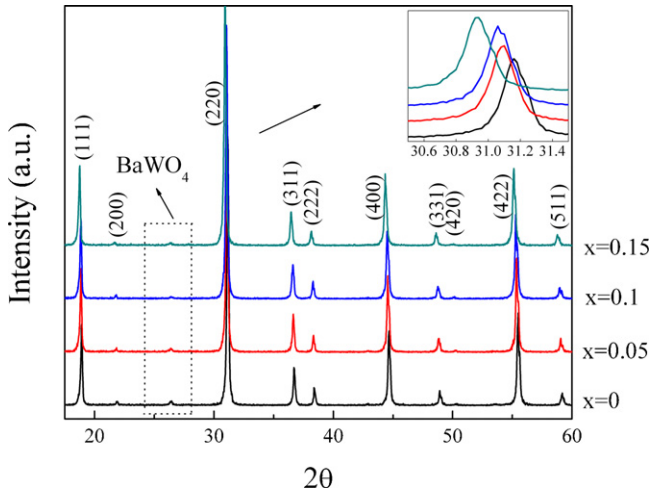

Fig. 1. Powder XRD patterns of $Ba_2Mg_{1-x}Ca_xWO_6$ sintered at 1500 °C/2 h.

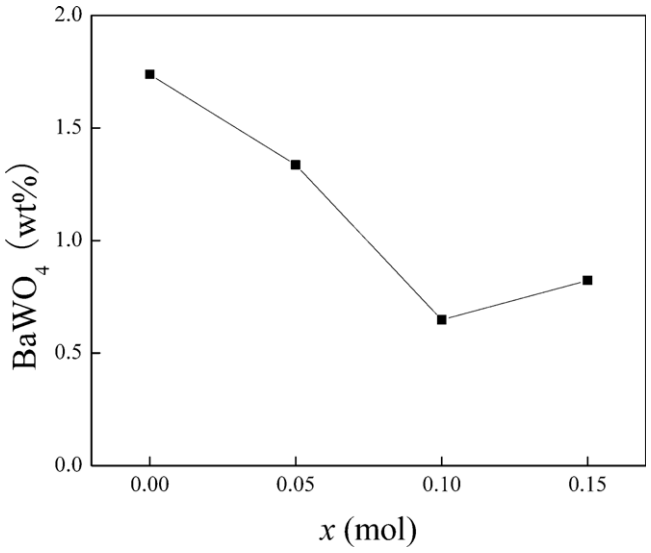

Fig. 2. Variation of $BaWO_4$ content with x of $Ba_2Mg_{1-x}Ca_xWO_6$ sintered at 1500 °C/2 h.

content again. In order to identify whether the $BaWO_4$ was originated from the incompletely reacted starting powders calcined at 1200 °C/2 h, Fig. 3 shows the powder XRD pattern of the calcined powders. No $BaWO_4$ or other impurity phases could be detected within its detecting limit. It clearly indicates that the presence of $BaWO_4$ in the sintered specimens should be caused by the thermal instability of $Ba_2Mg_{1-x}Ca_xWO_6$ compounds, which is in well agreement with that reported by Khalyvin et al. [11].

In order to clarify the variation of structural stability, the cubic structures of $Ba_2Mg_{1-x}Ca_xWO_6$ ceramics were further verified by the Rietveld refinement of the observed powder XRD profiles. $Fm-3m$ space group was proposed for all compositions. Linear interpolation between a set of background points with refinable heights was used to fit the background. The profiles were described using a Pseudo–Voigt function. In the initial refinements, the fractional occupancies of the B′ and B″-site cations were allowed to refine without any constraints, and their occupancies did not vary noticeably from 1, thus the fractional occupancies for all the B′ and B″-site cations were fixed to the stoichiometric composition. The impurity phase $BaWO_4$ was excluded in the refinement. The observed, calculated and difference profiles for the $x = 0.05$, $x = 0.1$ and $x = 0.15$ compositions are plotted in Fig. 4. Refined crystallographic results, main interatomic distances and bond valence are given in Tables 1 and 2, respectively.

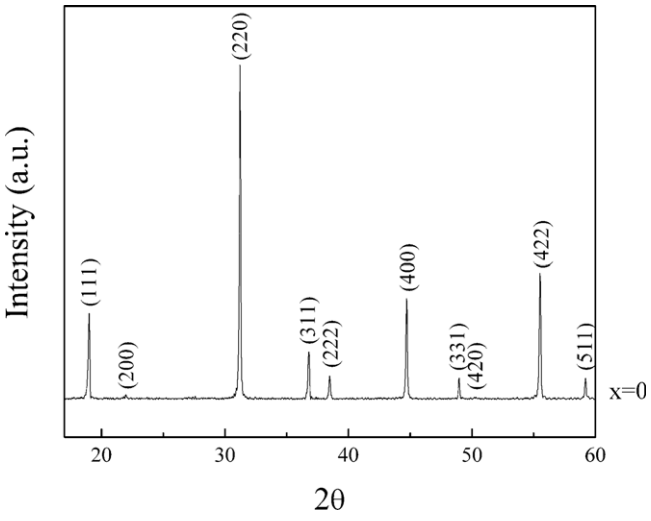

Fig. 3. Powder XRD pattern of Ba_2MgWO_6 calcined at 1200 °C/2 h.

For cubic double perovskites $Ba_2Mg\ WO_6$ ($Fm-3m$), Ba^{2+}, Mg^{2+} and W^{6+} remain on fixed Wyckoff positions: 8c (0.25, 0.25, 0.25), 4a (0, 0, 0) and 4b (0.5, 0.5, 0.5), respectively. The O^{2-} occupying 24e sites (x, 0, 0) can shift along the cell edge and adjust the interatomic distances between Mg^{2+} and W^{6+}

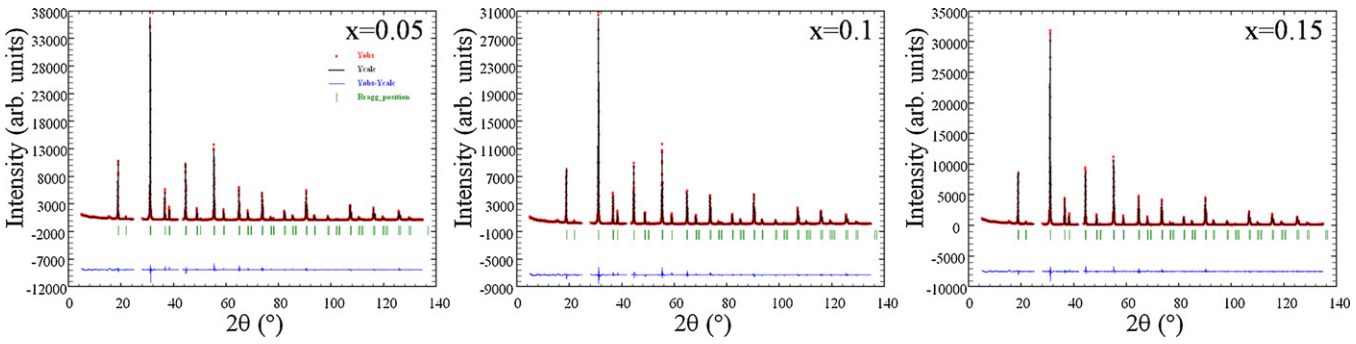

Fig. 4. Observed, calculated and difference profiles for the $x = 0.05$, $x = 0.1$ and $x = 0.15$ compositions.

Table 1
Atomic coordinates and thermal displacement parameters for $Ba_2Mg_{1-x}Ca_xWO_6$.

Composition	Atom	Site	*x/a*	*y/b*	*z/c*	U[a] Å^2	Occupancy
$x = 0.05$	Ba	8c	0.2500	0.2500	0.2500	0.09 (2)	0.33336
	Mg	4b	0.5000	0.5000	0.5000	0.84 (15)	0.15833
	Ca	4b	0.5000	0.5000	0.5000	0.84 (15)	0.00834
	W	4a	0.0000	0.0000	0.0000	−0.063 (16)	0.16667
	O	24e	0.2428 (6)	0.0000	0.0000	−0.00143, 0.00317, 0.00317	1.00000
$x = 0.10$	Ba	8c	0.2500	0.2500	0.2500	0.012 (21)	0.33336
	Mg	4b	0.5000	0.5000	0.5000	0.250 (131)	0.15000
	Ca	4b	0.5000	0.5000	0.5000	0.250 (131)	0.01667
	W	4a	0.0000	0.0000	0.0000	−0.190 (19)	0.16667
	O	24e	0.2479 (6)	0.0000	0.0000	−0.00143, 0.00317, 0.00317	1.00000
$x = 0.15$	Ba	8c	0.2500	0.2500	0.2500	0.047 (21)	0.33336
	Mg	4b	0.5000	0.5000	0.5000	0.358 (128)	0.14167
	Ca	4b	0.5000	0.5000	0.5000	0.358 (128)	0.02500
	W	4a	0.0000	0.0000	0.0000	−0.152 (18)	0.16667
	O	24e	0.2461 (6)	0.0000	0.0000	−0.00113, 0.00169, 0.00169	1.00000

[a] U_{iso} is listed for Ba, Mg/Ca, and W, and U_{11}, U_{22}, and U_{33} are listed for O.

cations. The O^{2-} anion is expected to move closer to the smaller, more highly charged W^{6+} due to Columbic forces. Thus Mg^{2+} is usually under bonded and W^{6+} over bonded. However the observed bond valences both of Mg (1.878 v.u.) and W (5.808 v.u.) are all under bonded due to the large tolerance factor of BMW ($t = 1.034$). Because for BMW with $t > 1$, the packing is determined by Ba^{2+} and B-site cations (Mg^{2+} and W^{6+}) have too much room. The over bonded Ba–O bond (2.496 v.u.) and weak Mg–O bond (1.878 v.u.) explains the instability of $Ba_2Mg\ WO_6$. It is noted that the Ba–O bond strength decreases monotonically with the increase of Ca substitution (Table 2); whereas the Mg/Ca–O bond strength increases with increasing Ca content up to $x = 0.10$ and then decreases again with further increase of x. The larger Ca^{2+} ion on Mg^{2+} lattice site may be expect to force the surrounding oxygen ion to expand so that the Mg/Ca–O distance would increase, as evidenced by the larger bond distance of Ca–O bond in Ba_2CaWO_6. However the resulting Mg/Ca–O distance decreases with increasing the Ca doping content. We suppose that this may be caused by a nonrandom distribution of Ca^{2+} and Mg^{2+} on 4b-site due to their large cation size difference ($R_{Mg^{2+}} = 0.72$ Å, $R_{Ca^{2+}} = 1.0$ Å), as it will be further confirmed later by Raman analysis. It is well known that XRD technique provides average structure information within long range scale for homogeneous materials. The local ordering between Mg and Ca cations on 4b-site will make refined atomic positions and resulting average bond length less credible. This may explain why the thermal displacement parameter of W^{6+} from the Rietveld refinement of the XRD data exhibits slight negative value. Therefore the resulting Mg/Ca–O and W–O bond lengths are less credible compared with that of Ba–O bond. In all cases, we think that the general varying trend for Mg/Ca–O bond valence is still credible by considering the Ca–O bond valence in Ba_2CaWO_6 (Table 2). The anomalous variation of Mg/Ca–O bond valence for $x - 0.15$ composition may be related to the local distribution between Ca and Mg cations. We believe that the decomposition of Ba_2MgWO_6 at higher temperature could be caused by the break of weak Mg–O

Table 2
Rietveld refinement results, bond distances, and bond valences from the X ray powder diffraction data of $Ba_2Mg_{1-x}Ca_xWO_6$.

Composition	$x = 0.00$[a]	$x = 0.05$	$x = 0.1$	$x = 0.15$	$x = 1.0$[a]
Volume (Å^3)	532.101 (4)	534.9781	537.6198	540.4292	590.26 (2)
a (Å)	8.10335 (2)	8.11793 (7)	8.13127(8)	8.14541 (9)	8.38843 (8)
R_{wp} (%)	2.33	12.3	12.4	12.0	10.48
R_p (%)	2.15	11.2	11.6	10.9	8.33
R_{exp} (%)	1.30	6.87	7.23	7.14	
Ba–O (Å) × 12	2.86665 (2)	2.871 (3)	2.875 (3)	2.880 (3)	2.9693 (3)
Mg/Ca–O (Å) × 6	2.1228 (6)	2.088 (5)	2.051 (5)	2.068 (5)	2.242 (7)
W–O (Å) × 6	1.9289 (6)	1.971 (5)	2.015 (5)	2.005 (5)	1.952 (7)
BVS(Ba)	2.496	2.464	2.436	2.403	1.89
BVS(Mg/Ca)[b]	1.878	2.142	2.460	2.436	2.85
BVS(W)	5.808	5.184	4.604	4.735	5.46
BVS(O)	1.961	2.048	2.001	2.012	2.01

[a] The structure refinement details for $x = 0.0$ and $x = 1.0$ composition is from reference [22] and [23], respectively.
[b] The average of Ro_{Ca} (1.693) and Ro_{Mg} (1.967) values was used for Ro [24].

Table 3
Bond valences of $Ba(Zn_{1/3}Nb_{2/3})O_3$, $Ba(Mg_{1/3}Ta_{2/3})O_3$ and $Ba(Zn_{1/2}W_{1/2})O_3$[a].

Composition	$Ba(Zn_{1/3}Nb_{2/3})O_3$	$Ba(Zn_{1/2}W_{1/2})O_3$	$Ba(Mg_{1/3}Ta_{2/3})O_3$
BVS(Ba)	2.258, 2.308	2.405	2.298, 2.413
BVS(B′)	1.720	1.866	1.938
BVS(B″)	5.055	5.88	4.794
BVS(O)	1.971, 2.133	2.107	2.071, 2.035

[a] The bond valence was calculated from the ICSD 157044, ICSD 240279 data and reference [25], respectively.

bond which resulted in the formation of $BaWO_4$. The decrease in $BaWO_4$ impurity phase with increasing Ca substitution could be mainly ascribed to the increase in Mg/Ca–O bond strength. This view could be generalized to the instability of other complex perovskites such as $Ba(Zn_{1/2}W_{1/2})O_3$, $Ba(Zn_{1/3}Nb_{2/3})O_3$ and $Ba(Mg_{1/3}Ta_{2/3})O_3$, in which barium tungstate, barium niobate and barium tantalate could be easily formed at high temperature, respectively. The instabilities of all above complex perovskites can also be attributed to the under-bonded B′–O bond (Table 3).

The presence of $BaWO_4$ in $Ba(Mg_{1/2}W_{1/2})O_3$ was also observed before [11,18]. The decomposition of Ba_2MgWO_6 could be considered as follows merely account for the mass balance:

$$Ba_2MgWO_6 \rightarrow BaWO_4 + BaO + MgO \quad (1)$$

or

$$Ba_2MgWO_6 \rightarrow (1/2)BaWO_4 + (1/2)Ba_3WO_6 + MgO \quad (2)$$

This means that there should also be BaO- and MgO-rich phase(s) present in the reaction mixture; however, neither BaO nor MgO was detected by X-ray diffraction. One possible reason for the absence of reflections of BaO phase in XRD could be ascribed to its amorphous state. Similar phenomenon is also observed for Ba_2ZnWO_6 [25], in which the decomposition is considered to be caused by the sublimation of ZnO above 1200 °C. In order to investigate the phase composition and assemblage of $Ba_2Mg_{1-x}Ca_xWO_6$ at high temperature, the SEM images and corresponding EDS analysis of the specimens sintered at 1500 °C/2 h are shown in Fig. 5. In all compositions, $BaWO_4$ precipitates are easily observed along the perovskite

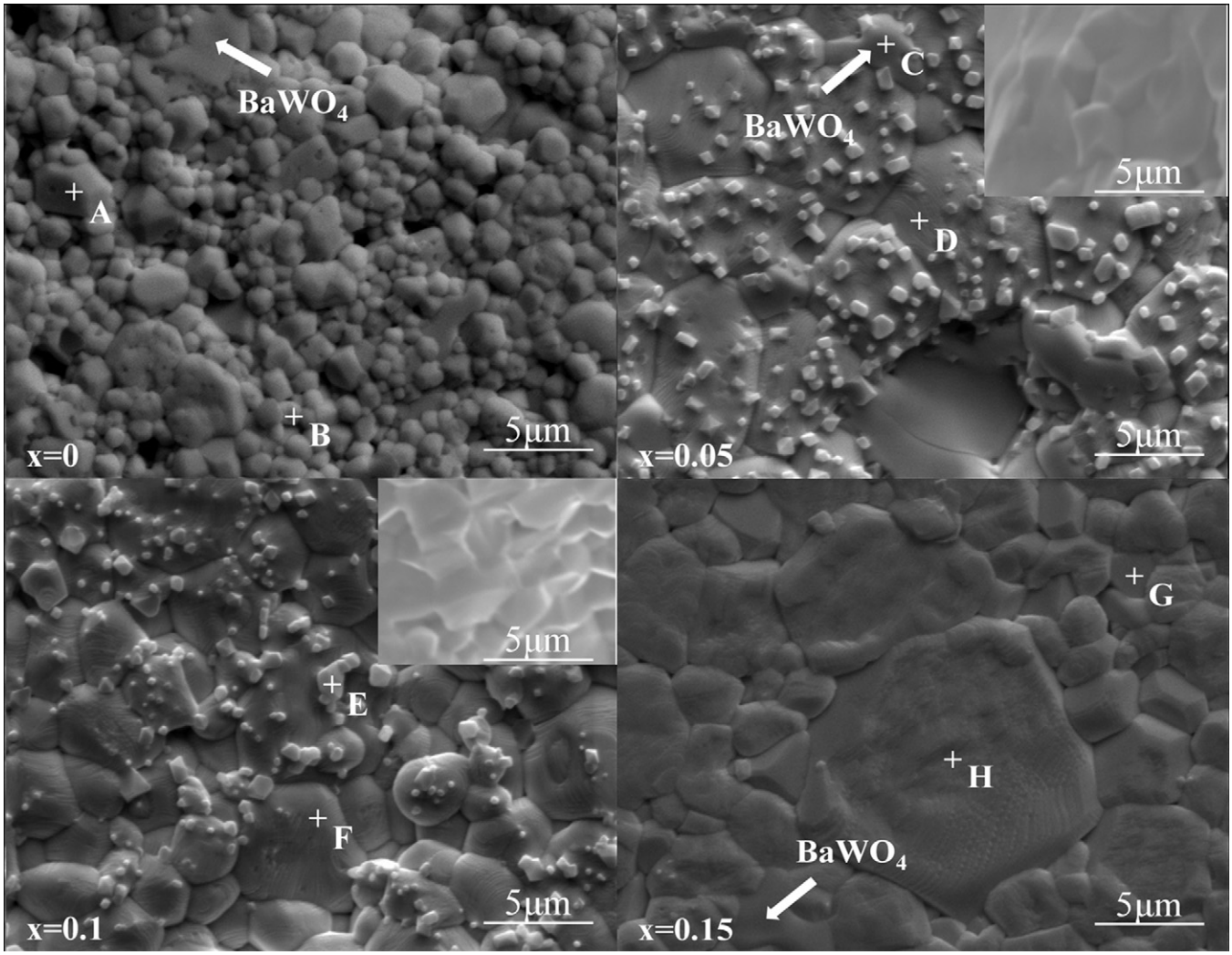

Fig. 5. (a) SEM images and (b) corresponding EDS analysis of the marked A–H spot in the specimens sintered at 1500 °C/2 h. The insets are SEM images of the fracture surface for $x = 0.05$ and $x = 0.1$ composition.

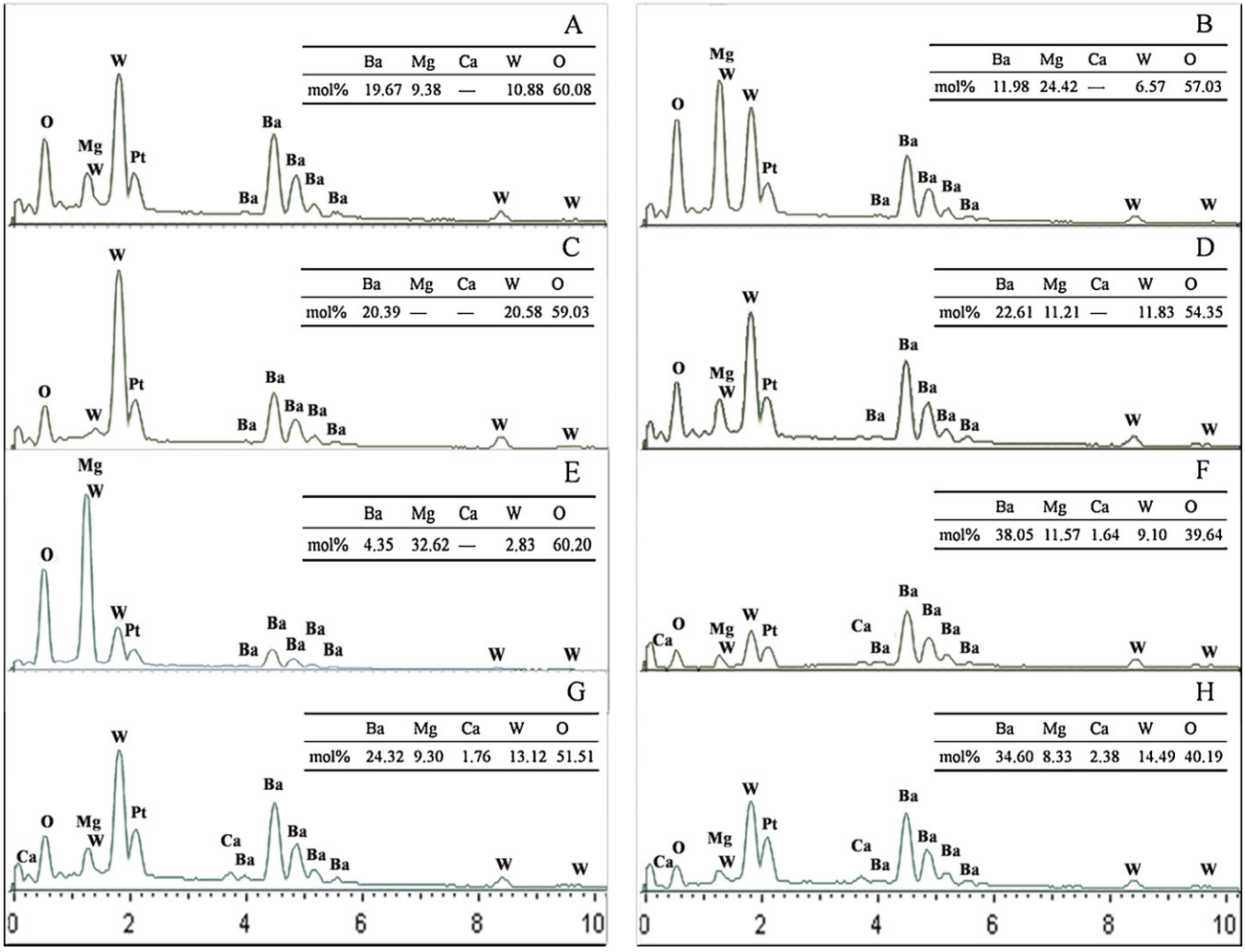

Fig. 5. (*Continued*).

matrix grain boundaries. For $x = 0$ composition, the round shaped grains indicates a typical liquid phase sintering due to the presence of $BaWO_4$ phase whose melting point (1430 °C) [26] is below the sintering temperature. As expected, Mg-rich phase is observed for all compositions by EDS analysis (marked B), although it was not detected by XRD analysis. It implies that the MgO-rich phase was in amorphous state. But it is noted that small white grains (~1 μm) precipitated on the surface of perovskite matrix grains for $x = 0.05$ and $x = 0.01$ compositions (marked E). EDS analysis shows that it was MgO-rich phase. However the SEM image of the fracture surface (see insets) shows no such kind of precipitates, which implies that the amorphous MgO-rich phase in $x = 0.05$ and $x = 0.01$ composition crystallized during the thermal etch process. The decomposition of Ba_2ZnWO_6 at high temperature is confirmed to be caused by the sublimation of ZnO due to its high partial pressure in air [25]. However, in the case of Ba_2MgWO_6, the vaporization rate of MgO should be much slower compared with that of ZnO because the partial pressure of Mg in air is much lower than that of Zn [27]. This explained the existence of amorphous MgO-rich phase in $Ba_2Mg_{1-x}Ca_xWO_6$ ceramics. Unexpectedly, the amorphous BaO-rich phase is not observed in SEM image for all composition, which provides clues for the evaporation of Ba-rich species at high temperature or remained as an amorphous state, although it should be further confirmed by TEM analysis. Considering the high temperature vaporization behavior for BaO, MgO/CaO [27], and phase equilibrium over $BaO–WO_3$ solids and liquids [28], noteworthy is the obvious fact the vaporization rate of BaO is much larger than that of MgO/CaO and $BaWO_4$. Therefore Ba-rich species dominate the vapor over compositions richer in BaO than $BaWO_4$, e.g. Ba_3WO_6. The vaporization of Ba species in $Ba(Mg_{1/3}Ta_{2/3})O_3$ system has been confirmed by the fact that BaO content in the $Ba(Mg_{1/3}Ta_{2/3})O_3$ powders sintered at 1600 °C decreases with increasing soaking time [29]. However the vaporization of Ba-rich species directly from $Ba(Mg_{1/3}Ta_{2/3})O_3$ or $Ba_2Mg_{1-x}Ca_xWO_6$ matrix seems to be neglected due to the strongly over-bonded Ba–O bond as discussed above. However the vaporization of Ba-rich species would increase considerably if BaO phase formed as result of the decomposition of $Ba(Mg_{1/3}Ta_{2/3})O_3$ or $Ba_2Mg_{1-x}Ca_xWO_6$ due to the weak Mg/Ca–O bond. The vaporization of Ba-rich species from BaO or Ba_3WO_6, on the other hand, would in turn facilitate the decomposition of $Ba_2Mg_{1-x}Ca_xWO_6$

according to the mass balance equation (1) or (2). In this case, there would be no need to infer that BaO-rich phases must be present. Summary, the scenario of the difficult synthesis, structural instability and thermodynamic decomposition of Ba_2MgWO_6 at high temperature could be described as follows: the larger enthalpy of $BaWO_4$ compared with that of $MgWO_4$ is responsible for the preferential formation of $BaWO_4$ during synthesizing process, which makes it difficult to get a pure Ba_2MgWO_6. Although pure Ba_2MgWO_6 can be obtained by well processed synthesis, e.g. stepwise process, the under-bonded Mg–O bond destabilizes the double perovskite structure at higher temperature. BaO-rich phase forms as result of the thermal decomposition of Ba_2MgWO_6, which easily vaporizes at high temperature. The vaporization of BaO-rich phase, in turn, facilitates the decomposition of Ba_2MgWO_6 and shift bulk composition chemistries toward the WO_3-richer portion of the system, which would produce more secondary phases including $BaWO_4$ and MgO according to the mass balance equation. The doping of Ca on Mg-site increases the Mg/Ca–O bond strength, thus the thermal structural stability of $Ba_2Mg_{1-x}Ca_xWO_6$, which restrains the formation of BaO-rich phase. Therefore the formation of BaO-rich phase and its high vaporization rate at high temperature justified the phase assemblage observed for $Ba_2Mg_{1-x}Ca_xWO_6$ ceramics sintered at 1500 °C/2 h. For the Zn-containing complex perovskites, the weak Zn–O bond and high vaporization rate of Zn species make the decompositions of perovskites directly from the breaking of Zn–O bond and sublimation of ZnO even though ZnO-rich phase does not form first. This may explain why BaO-rich phase rather than ZnO-rich phase could be observed in Ba_2ZnWO_6 ceramics, whereas MgO-rich phase rather than BaO-rich phase could be detected in $Ba_2Mg_{1-x}Ca_xWO_6$ ceramics.

Raman spectroscopy is considered to be more powerful than XRD analysis for probing the local crystal structure. Fig. 6 shows the Raman spectra of $Ba_2Mg_{1-x}Ca_xWO_6$ ceramics. The 1:1 ordered perovskites with the $Fm-3m$ symmetry allow the

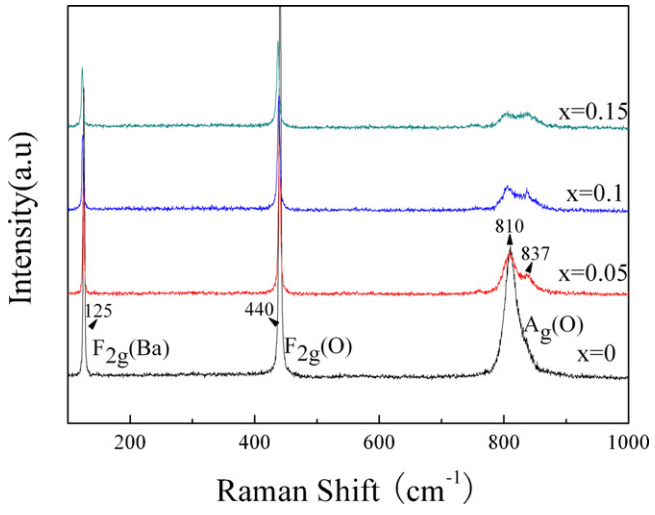

Fig. 6. Raman spectra of $Ba_2Mg_{1-x}Ca_xWO_6$ ceramics sintered at 1500 °C/2 h.

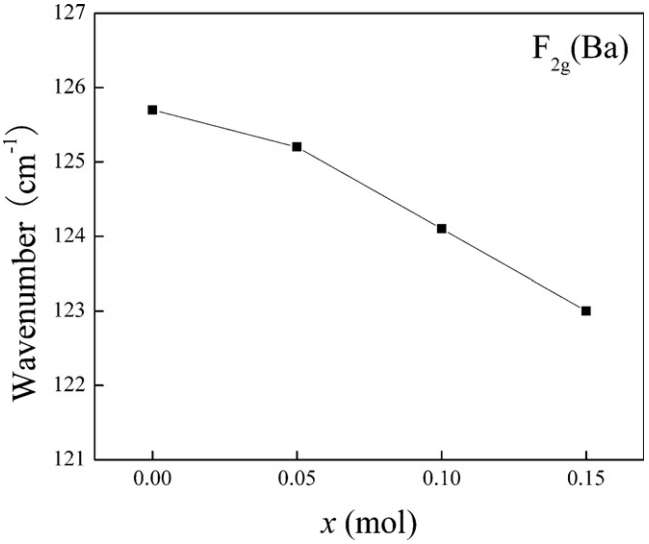

Fig. 7. Raman shift as function of x.

appearance of four Raman-active modes ($\Gamma = A_{1g}(O) + E_g(O) + F_{2g}(O) + F_{2g}(Ba)$) [30]. However, as can be seen in Fig. 6, three main modes are observed for all specimens, which is consistent with the observations for other 1:1 ordered perovskites. The band centered at around 810 cm^{-1} could be attributed to $A_{1g}(O)$ mode which corresponds to the symmetric breath-type stretching vibration of oxygen octahedron. The band at 125 cm^{-1} and 440 cm^{-1} could be ascribed to triple degenerate $F_{2g}(Ba)$ and $F_{2g}(O)$ modes, respectively. The E_g mode here is too weak to be detected. It is noted that the intensity of the $A_{1g}(O)$ mode at 810 cm^{-1} decreases and a new weak band emerges at about 837 cm^{-1} with the increase of Ca substitution, which is in agreement with the observation of Blasse [21]. According to Blasse's analysis, the former was ascribed to the mode of a WO_6 octahedron surrounded by six Mg^{2+} ions, and the new band at 840 cm^{-1} was assigned to the mode of a WO_6 octahedron surrounded by five Mg^{2+} ions and one Ca^{2+} ion. It implies a nonrandom distribution of Ca^{2+} and Mg^{2+} on 4b-site within the short range scale due to their large cation size difference as discussed above. Notably, The $F_{2g}(Ba)$ mode shifts slightly to lower frequency with the increase of Ca-substitution (Fig. 7). The red shifted $F_{2g}(Ba)$ could be associated with decrease of the Ba–O bond strength with increasing Ca substitution (Table 2).

Variation of dielectric permittivity as function of Ca substitution is shown in Fig. 8. The dielectric permittivity increases with the increase of Ca substitution. The increase in dielectric permittivity could be related to the increase in ionic polarizability of B′-site cation ($\alpha_{Ca^{2+}} = 3.16\,(Å^3)$, $\alpha_{Mg^{2+}} = 1.32\,(Å^3)$) [31] and decrease of Ba–O bond strength, although the cell volume increased simultaneously with the increase of Ca substitution. Fig. 9 illustrates the variation of $Q \times f$ value with Ca substitution. Small amount of Ca-doping ($x < 0.1$) did not affect the optimized $Q \times f$ value greatly. The maximum $Q \times f$ value of about 124,000 GHz could be obtained at $x = 0.05$ composition. It is well known that for 1:1 ordered perovskites, the intrinsic dielectric loss is mainly dominated by

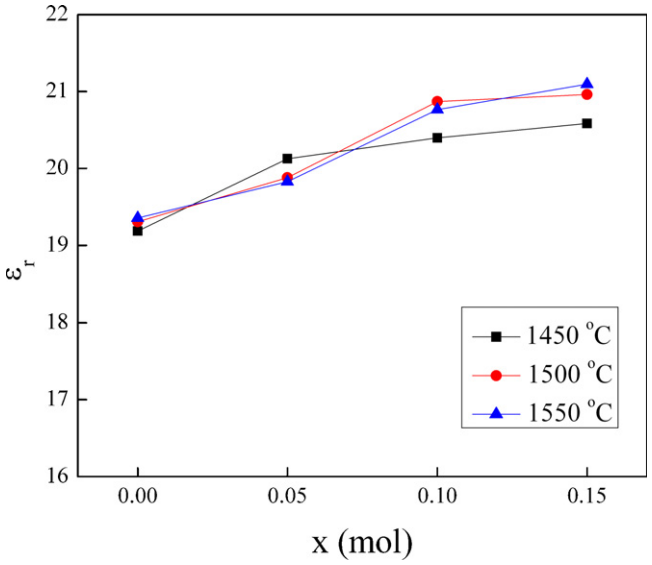

Fig. 8. Variation of dielectric permittivity of $Ba_2Mg_{1-x}Ca_xWO_6$ ceramic as function of x.

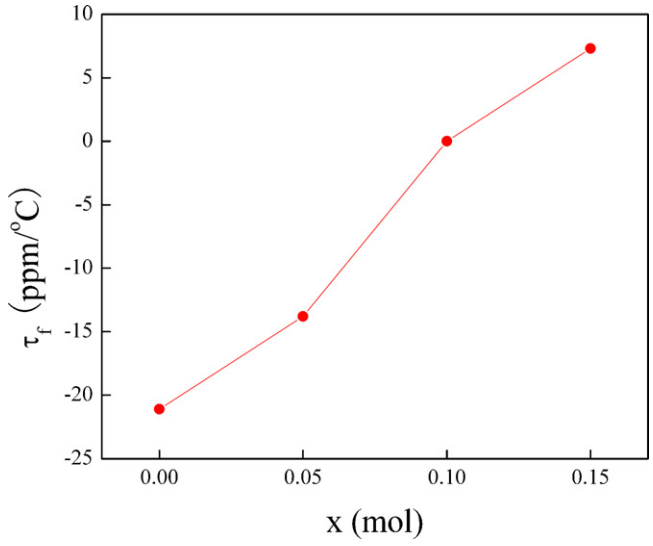

Fig. 10. Variation of τ_f value with x.

low frequency modes corresponding to A-BO_6 vibrations and B-O_6 stretching vibration, respectively [19]. For Ba_2MgWO_6 ($x = 0$), it is the over-bonded Ba–O bond which makes it possess higher $Q \times f$ value than that of Sr_2MgWO_6 and Ca_2MgWO_6 in which case the A–O bond strength decreases as the sequence of Sr and Ca series. The second mode is sensitive to B′-site cation. Therefore the increase in Mg/Ca–O bond strength with Ca-substitution is expected to increase the intrinsic $Q \times f$ value of $Ba_2Mg_{1-x}Ca_xWO_6$ ceramic, while the decrease in Ba–O bond strength has opposite effect on the $Q \times f$ value. The total intrinsic $Q \times f$ value of $Ba_2Mg_{1-x}Ca_xWO_6$ ceramic was dominated by the two competing factors. Thus the slight decrease in $Q \times f$ value when $x \geq 0.1$ could be ascribed to the dominating factor of decrease in Ba–O bond strength. Extrinsic factors such as impurity phases, pores and boundaries also contribute to the dielectric loss. In the case of $Ba_2Mg_{1-x}Ca_xWO_6$ ceramics, porosity is low as shown in Fig. 5. So the effect of porosity on the $Q \times f$ value could be neglected. The influence of $BaWO_4$ and MgO impurity phases on the $Q \times f$ value is manifested by the decrease in $Q \times f$ value from ~120,000 to ~20,000 GHz when the samples were stored under ambient conditions for a long time. We believe that this deterioration might be caused by the hygroscopy of MgO in the air humidity. The deterioration in $Q \times f$ value depends on the content of MgO impurity phases and humidity in the environment. Complete suppression of the decomposition of BMW is therefore of crucial importance for practical application. As expected, the doping of Ca tunes the temperature coefficient of resonant frequency (τ_f value) from negative to positive value (Fig. 10). Zeroτ_f value could be obtained at $x = 0.1$ composition.

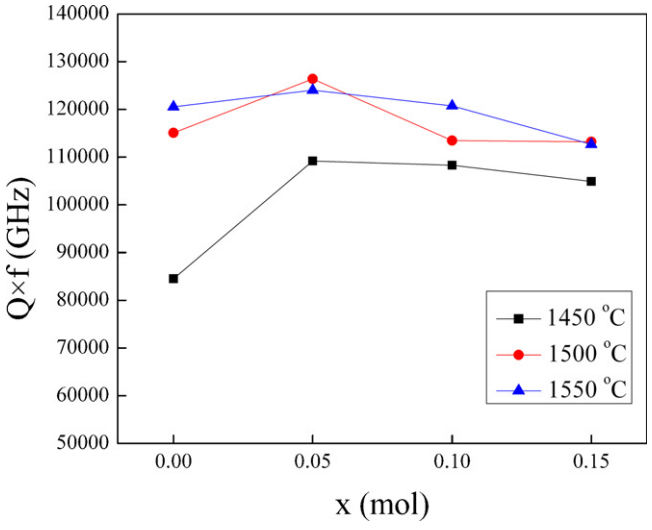

Fig. 9. Variation of $Q \times f$ value of $Ba_2Mg_{1-x}Ca_xWO_6$ ceramic with x.

4. Conclusions

The structure stability and microwave dielectric properties of double perovskite ceramics – $Ba_2Mg_{1-x}Ca_xWO_6$ ($0.0 \leq x \leq 0.15$) have been studied in this paper. The weak Mg–O bond causes the decomposition of Ba_2MgWO_6 at high temperature, which results in the formation of $BaWO_4$ and amorphous MgO. Small amount of Ca substitution for Mg increases the Mg/Ca–O bond strength, and hence the stability of the double perovskite. But it cannot completely suppress the decomposition of $Ba_2Mg_{1-x}Ca_xWO_6$ at high temperature. Although the doped specimens exhibit the same face cubic phase as undoped specimen, nonrandom distribution of Ca^{2+} and Mg^{2+} on 4b-site within the short range scale is observed due to their large cation size difference. Small level doping of Ca ($x \leq 0.1$) increases the dielectric permittivity monotonically, but does not affect the $Q \times f$ value greatly. As expected, the doping of Ca tuned the temperature coefficient of resonant frequency (τ_f value) from negative to positive value. Zero τ_f value could be obtained for $x = 0.1$ composition. Excellent combined microwave dielectric properties with $\varepsilon_r = 20.8$, $Q \times f = 120{,}729$ GHz, and $\tau_f = 0$ ppm/°C could be obtained

for $x = 0.1$ composition; however the remained amorphous MgO in $Ba_2Mg_{1-x}Ca_xWO_6$ ceramic decrease its $Q \times f$ value considerably when the sample was stored under ambient conditions for a long time due to the hygroscopy of MgO in the air humidity. Complete suppression of the decomposition of BMW is therefore of crucial importance for practical application.

References

[1] S. Nomura, K. Toyama, K. Kaneta, $Ba(Mg_{1/3}Ta_{2/3})O_3$ ceramics with temperature-stable high dielectric constant and low microwave loss, Jpn. J. Appl. Phys. 21 (1982) L624–L626.

[2] S. Kawashiima, M. Nishida, I. Ueda, H. Ouchi, $Ba(Zn_{1/3}Ta_{2/3})O_3$ ceramics with low dielectric loss at microwave frequencies, J. Am. Ceram. Soc. 66 (1983) 421–423.

[3] S.B. Desu, O'Bryan, Microwave loss of $Ba(Zn_{1/3}Ta_{2/3})O_3$ ceramics, J. Am. Ceram. Soc. 68 (1985) 546–551.

[4] P.K. Davies, J. Tong, T. Negas, Effect of ordering-induced domain boundaries on low-loss $Ba(Zn_{1/3}Ta_{2/3})O_3$–$BaZrO_3$ perovskite microwave dielectrics, J. Am. Ceram. Soc. 80 (1997) 1727–1740.

[5] J.I. Yang, S. Nahn, C.H. Choi, H.J. Lee, H.M. Park, Microstructure and microwave dielectric properties of $Ba(Zn_{1/3}Ta_{2/3})O_3$ ceramics with ZrO_2 addition, J. Am. Ceram. Soc. 85 (2002) 165–168.

[6] R.I. Scott, M. Rhomas, C. Hampson, Development of low cost, high performance $Ba(Zn_{1/3}Nb_{2/3})O_3$ based materials for microwave resonator applications, J. Eur. Ceram. Soc. 23 (2003) 2467–2471.

[7] M. Takata, K. Kageyama, Microwave characteristics of $A(B^{3+}{}_{1/2}B^{5+}{}_{1/2})O_3$ ceramics (A = Ba, Ca, Sr; B^{3+} = La, Nd, Sm, Yb; B^{5+} = Nb, Ta), J. Am. Ceram. Soc. 72 (1989) 1955–1959.

[8] L. Abdul Khalam, S. Thomas, M.T. Sebastian, Temperature-stable and low-loss dielectrics in the $Ca(B'_{1/2}Ta_{1/2})O_3$ B′ = Lanthanides, Y, and In System, J. Am. Ceram. Soc. 90 (2007) 2476–2483.

[9] A. Dias, M.M. Lage, L.A. Khalam, M.T. Sebastian, R.L. Moreira, Vibrational spectroscopy of Ca_2LnTaO_6 (Ln = lanthanides, Y, and In) and Ca_2 $InNbO_6$ double perovskites, Chem. Mater. 23 (2011) 14–20.

[10] M. Takata, K. Kageyama, Microwave characteristics of $A(B^{3+}{}_{1/2}$ $B^{5+}{}_{1/2})O_3$ ceramics, J. Am. Ceram. Soc. 72 (1989) 1955–1959.

[11] D.D. Khalyvin, J. Han, A.M.R. Senos, P.Q. Mantas, Synthesis and dielectric properties of tungsten-based complex perovskites, J. Mater. Res. 1811 (2003) 2600–2607.

[12] A. Salinas-Sanchez, J.L. Garcia-Munoz, J. Rodriguez-Carvajal, R. Saez-Puche, J.L. Martinez, Structural characterization of R_2 $BaCuO_5$ (R = Y, Lu, Yb, Tm, Er, Ho, Dy, Gd, Eu and Sm) oxides by X-ray and neutron diffraction, J. Solid State Chem. 100 (2) (1992) 201–211.

[13] W. Lufaso Michael, M. Woodward Patrick, Prediction of the crystal structures of perovskites using the software program SPuDS, Acta Crystallogr. B57 (2001) 725–738.

[14] Q. Guo, O. Jakob, Enthalpies of formation from the component oxides of $MgWO_4$, $CaWO_4$ (scheelite), $SrWO_4$, and $BaWO_4$, determined by high-temperature direct synthesis calorimetry, Thermochim. Acta 288 (1996) 53–61.

[15] F. Zhao, Z.X. Yue, Z.L. Gui, L.T. Li, Preparation, characterization and microwave dielectric properties of A_2, BWO_6 (A = Sr, Ba; B = Co, Ni, Zn) double perovskite ceramics, Jpn. J. Appl. Phys. 44 (2005) 8066–8070.

[16] H. Takahashi, K. Ayusawa, N. Sakamoto, Microwave dielectric properties of $Ba(Mg_{1/2}W_{1/2})O_3$–$BaTiO_3$ ceramics, Jpn. J. Appl. Phys. 36 (1997) 5597–5599.

[17] D.D. Khalyavin, A.M.R. Senos, P.Q. Mantas, 6H hexagonal structure of low loss Ba_3MTiWO_9 (M = Mg, Zn) dielectrics, Mater. Res. Bull. 42 (2007) 126–130.

[18] J.J. Bian, K. Yan, Y.F. Dong, Microwave dielectric properties of $A_{1-3x/2}La_x(Mg_{1/2}W_{1/2})O_3$ (A = Ba, Sr, Ca; $0.0 \leq x \leq 0.05$) double perovskites, Mater. Sci. Eng. B 147 (2008) 27–34.

[19] R. Zurmuhlen, J. Petzelt, S. Kamba, V.V. Vooitsekhovskii, E. Colla, N. Setter, Dielectric spectroscopy of $Ba(B'_{1/2}B'_{1/2})O_3$ complex perovskite ceramics: relations between ionic parameters and microwave dielectric properties. I. Infrared reflectivity study (10^{12}–10^{14}Hz), J. Appl. Phys. 77 (10) (1995) 5341–5350.

[20] Y.Y. Zhou, S.Q. Meng, H.C. Wu, Z.X. Yue, Microwave dielectric properties of $Ba_2Ca_{1-x}Sr_xWO_6$ double perovskites, J. Am. Ceram. Soc. (2011) 1–6.

[21] G. Blasse, Vibrational spectra of solid solution series with ordered perovskite structure, J. Inorg. Nucl. Chem. 37 (1975) 1347–1351.

[22] H.W. Eng, The crystal and electronic structures of oxides containing d0 transition metals in octahedral coordination, PhD Thesis, Ohio State University, USA, (2003)

[23] D.E. Bugaris, J.P. Hodges, A. Huq, H.C. Loye, Crystal growth, structures, and optical properties of the cubic double perovskites Ba_2MgWO_6 and Ba_2ZnWO_6, J. Solid State Chem. 184 (2011) 2293–2298.

[24] D. Brown, D. Altermatt, Bond-valence parameters obtained from a systematic analysis of the inorganic crystal structure database, Acta Crystallogr. B41 (1985) 244–247.

[25] B. Jancarw, J. Bezjak, P.K. Davies, High-temperature decomposition of B-site-ordered perovskite $Ba(Zn_{1/2}W_{1/2})O_3$, J. Am. Ceram. Soc. 93 (3) (2010) 758–764.

[26] L.L.Y. Chang, M.G. Scroger, B. Phillips, Alkaline–earth tungstates: equilibrium and stability in the M–W–O systems, J. Am. Ceram. Soc. 49 (7) (1966) 385–390.

[27] R.H. Lamoreaux, D.L. Hildenbrand, L. Brewer, High temperature vaporization behavior of oxides II. Oxides of Be, Mg, Ca, Sr, Ba, B, Al, Ga, In, Tl, Si, Ge, Sn, Pb, Zn, Ca and Hg, J. Phys. Chem. Ref. Data 163 (1997) 419–433.

[28] E.R. Kreidler, Phase equilibrium in the system of calcium oxide–barium oxide–tungsten oxide, J. Am. Ceram. Soc. 55 (10) (1972) 514–519.

[29] J.J. Bian, Study on the high-Q $Ba(Mg_{1/3}Ta_{2/3})O_3$ microwave dielectrics, PhD Thesis, Shanghai Institute of Ceramics, Chinese Academy of Science, China, (1998)

[30] I.G. Siny, R. Tao, R.S. Katiyar, R.Y. Guo, A.S. Bhalla, Raman spectroscopy of Mg–Ta order–disorder in $BaMg_{1/3}Ta_2/3O_3$, J. Phys. Chem. Solid 59 (1998) 181–195.

[31] V.J. Fratello, C.D. Brandle, Calculation of dielectric polarizabilities of perovskite substrate materials for high-temperature superconductors, J. Mater. Res. 910 (1994) 2554–2559.